
MULTI-VIEW DATA VISUALISATION VIA MANIFOLD LEARNING

Theodoulos Rodosthenous*
Department of Mathematics
Imperial College London
London, SW7 2AZ, UK
tr1915@ic.ac.uk

Vahid Shahrezaei
Department of Mathematics
Imperial College London
London, SW7 2AZ, UK
v.shahrezaei@imperial.ac.uk

Marina Evangelou
Department of Mathematics
Imperial College London
London, SW7 2AZ, UK
m.evangelou@imperial.ac.uk

October 20, 2021

ABSTRACT

Manifold learning approaches, such as Stochastic Neighbour Embedding (SNE), Locally Linear Embedding (LLE) and Isometric Feature Mapping (ISOMAP) have been proposed for performing non-linear dimensionality reduction. These methods aim to produce two or three latent embeddings, in order to visualise the data in intelligible representations. This manuscript proposes extensions of Student's t-distributed SNE (t-SNE), LLE and ISOMAP, to allow for dimensionality reduction and subsequent visualisation of *multi-view* data.

Nowadays, it is very common to have multiple data-views on the same samples. Each data-view contains a set of features describing different aspects of the samples. For example, in biomedical studies it is possible to generate multiple OMICS data sets for the same individuals, such as transcriptomics, genomics, epigenomics, enabling better understanding of the relationships between the different biological processes.

Through the analysis of real and simulated datasets, the visualisation performance of the proposed methods is illustrated. Data visualisations have been often utilised for identifying any potential clusters in the data sets. We show that by incorporating the low-dimensional embeddings obtained via the *multi-view manifold learning* approaches into the K-means algorithm, clusters of the samples are accurately identified. Our proposed multi-SNE method outperforms the corresponding multi-ISOMAP and multi-LLE proposed methods. Interestingly, multi-SNE is found to have comparable performance with methods proposed in the literature for performing multi-view clustering.

Keywords Multi-view Data · Data Visualisation · Manifold Learning · Clustering

1 Introduction

In recent years, scientists in many fields generate multiple data-views on the same samples, referred to as *multi-view data*. Images can be represented differently according to their color, projection or texture [Chua et al., 2009], while OMICS data in biomedical studies quantify different aspects of an organism's biological processes [Hasin et al., 2017]. Real multi-view data are often classified as heterogeneous, as each data-view has its own distribution and variation pattern Rodosthenous et al. [2020].

Several approaches have been proposed over the years for the analysis of multi-view data. They include techniques on clustering [Ye et al., 2018, Ou et al., 2018], classification [Shu et al., 2019], regression [Li et al., 2019], dimensionality reduction [Sun, 2013] and more [Xu et al., 2013, Zhao et al., 2017]. However, the literature mostly lacks efficient algorithms that allow the construction of a single visualisation, through the simultaneous analysis of multiple data-views. Most existing methods can produce multiple visualisations (one from each view) or combine the features of the data-views prior to visualising the data. Having a single visualisation is very beneficial in the analysis of multi-view data, as it provides a global overview of the data and reveals patterns that would potentially be missed by looking at the data-views separately.

*Contact author

In order to create a comprehensible projection of high-dimensional data, we need to have two or three latent embeddings that capture the underlying structure of the data. This is the specific goal of *manifold learning*, an active research area within machine learning, which aims to perform non-linear dimensionality reduction. By assuming that the dimensions of the data sets are artificially high, manifold learning methods aim to capture important information in an induced low-dimensional embedding [Zheng and Xue, 2009]. Such low-dimensional embeddings can be used for visualisation purposes.

In this work, we propose different solutions to multi-view manifold learning based on existing algorithms that find latent embeddings of single-view data. Such methods focus on preserving at least one of the characteristics of the data. For example, the Stochastic Neighbour Embedding (SNE) [Hinton and Roweis, 2003] preserves the probability distribution of the data. The Locally Linear Embedding (LLE) proposed by Roweis and Saul [2000] is a neighbourhood-preserving method. The Isometric Feature Mapping (ISOMAP) proposed by [Tenenbaum et al., 2000] is a quasi-isometric method based on Multi-Dimensional Scaling [Groenen and Borg, 2013]. Spectral Embeddings [Ng et al., 2001] finds low-dimensional embeddings via spectral decomposition of the Laplacian matrix. The Local Tangent Space Alignment method proposed by [Zhang and Zha, 2004] learns the embedding by optimising local tangent spaces representing the local geometry of each neighbourhood and UMAP [McInnes et al., 2018] preserves the global structure of the data by constructing a theoretical framework based in Riemannian geometry and algebraic topology.

Most manifold learning algorithms have been proposed for the analysis of single-view data. Thus researchers often rely on visualising each data-view separately or concatenating features of multiple data-views to a single data set. The former could provide misleading outcomes, with each data-view revealing different visualisations and patterns. The different statistical properties, physical interpretation, noise and heterogeneity between data-views suggest that concatenating features would often fail in achieving a reliable interpretation and visualisation of the data [Fu et al., 2008]. The focus of this manuscript is the analysis of multi-view data through manifold learning methods, a challenging topic that has not been widely addressed in the literature, except in some studies as discussed in the following.

Xie et al. [2011] proposed such a solution, called multi-view Stochastic Neighbour Embedding (m-SNE). It combines the probability distributions produced by each data-view into a single distribution through a weight parameter. M-SNE then implements the solution by t-SNE on the combined distribution to obtain a single low-dimensional embedding. The algorithm finds the optimal choice for both the low-dimensional embeddings and the weight parameter simultaneously. In contrast, we propose *multi-SNE*, an extension of t-SNE that produces low-dimensional embeddings by integrating the information encoded in the multiple data-views iteratively, resulting in a different cost function and more robust solutions than m-SNE.

Multi-view Locally Linear Embeddings (m-LLE) [Shen et al., 2013] is an extension of LLE and it was primarily developed to effectively retrieve medical images. m-LLE produces a single low-dimensional embedding by integrating the embeddings from each data-view according to a weight parameter c , which refers to the contribution of each data-view. Similarly to m-SNE, the algorithm optimizes both the weight parameter and the embeddings simultaneously. Here, we propose a separate solution based on LLE, called *multi-LLE*, which uses a consensus weight matrix prior to computing the low-dimensional embeddings. Further, by using a similar methodology, we developed a modification of ISOMAP, called *multi-ISOMAP*, that allows multi-view data as input.

Other existing non-linear multi-view manifold learning algorithms aim to reduce the dimensions of the data, but not solely to produce a good single visualisation. Multi-view Manifold Learning with Locality Alignment (MVML-LA) [Zhao et al., 2018] learns a discriminative common low-dimensional latent space by assuming that each data-view is generated through that latent space and a generation function. The implementation of locality alignment constraint enhances the discriminant ability of the latent space. Multi-view Intact Space Learning (MISL) [Xu et al., 2015] discovers a latent intact representation by integrating encoded information from multiple data-views. MVML-LA and MISL are not often used to visualise the data, and they have not been examined in this paper.

The outcome of linear and non-linear dimensionality reduction methods can be used as input variables in other machine learning algorithms for the modelling. For example, LLE has been applied for classification [de Ridder et al., 2003], regression [Xiang et al., 2011], feature extraction [Li et al., 2016], and clustering [Hui and Wang, 2008]. Yu et al. [2012] and Li et al. [2017] have used ISOMAP for clustering and classification, respectively. Alternatively, t-SNE is seen solely as a data visualisation technique. Schubert and Gertz [2017] argue that t-SNE should not be used for clustering or outlier detection, since the latent embeddings do not preserve distances or densities well. In this work, we show that this is not always true.

Data visualisation communicates relationships between the data through intelligible representations. A common example of such relationships is when data points are separated into clusters. The data sets used in this manuscript allow for this type of communication, as they have been previously used in studies that tackle multi-view clustering. This property of the data was taken as the basis of our evaluation process. Motivated by Linderman and Steinerberger

[2019], who demonstrated that t-SNE often recovers well-separated clusters of data, we applied K-means on the low-dimensional embeddings and evaluated their performance through common clustering measures. This process was performed on two real data sets, one having perfectly balanced labels and the second imbalanced. We show that this approach produces results comparable to those obtained by implementing multi-view clustering algorithms.

The focus of this paper, is the creation of visualisations of multi-view data in a single figure, by modifying t-SNE, LLE and ISOMAP. In Section 2 we present the multi-view manifold learning algorithms, based on t-SNE (Section 2.3), LLE (Section 2.4) and ISOMAP (Section 2.5). In Section 3, we present the results of these algorithms implemented on five data sets, two of which were synthetically generated. We discuss our conclusions in Section 4.

2 Multi-view Manifold Learning

In this section, we present our proposed methods. After the notation is explained in Section 2.1, a toy example that will be referred to throughout this section is described in Section 2.2. Multi-SNE, multi-LLE and multi-ISOMAP are introduced in Sections 2.3, 2.4 and 2.5, respectively.

2.1 Notation

Throughout this paper, we use the following notation:

- $X \in \mathbb{R}^{N \times p}$: A single-view data matrix, representing the original high-dimensional data used as input; \mathbf{x}_i is the i^{th} data point of X .
- $X^{(m)} \in \mathbb{R}^{N \times p_m}$: The m^{th} data-view of multi-view data; \mathbf{x}_i^m is the i^{th} data point of $X^{(m)}$.
- $Y \in \mathbb{R}^{N \times d}$: A low-dimensional embedding of the original data. Since this paper’s focus is on data visualisation, usually $d = 2$; \mathbf{y}_i is the i^{th} data point of Y .

2.2 Toy Example Description

A motivational toy example was generated to highlight the ability of multi-view manifold learning techniques in combining information from multiple data-views. A comparison against single-view visualisations highlights the benefits of performing multi-view visualisations.

Suppose that for the same samples, three data-views are available, with each data-view capturing different information of the samples. The data were generated as follows. Each sample follows a normal distribution with mean μ and standard deviation $\sigma = 1$. For each data-view, different μ values were chosen to distinguish the clusters. Noise, following a normal distribution with mean $\mu_\epsilon = 0$ and standard deviation $\sigma_\epsilon = 1$, was added to increase randomness within each data-view. Polynomial functions were then applied on the samples to express non-linearity. The last step was performed to ensure that linear dimensionality reduction methods (*e.g.* PCA) would not successfully cluster the data.

Assume that the data are separated into three true clusters as presented in Figure 1. Implementing single-view manifold learning algorithms result in three distinct clusterings, none of which reflects the truth. In particular, the first view separates only cluster **C** from the others (view 1), the second view separates only cluster **B** (view 2) and the third view separates only cluster **A** (view 3). Throughout this section, we examine whether the proposed multi-view manifold learning algorithms capture the underlying structure of the data and separate the data points to the true three clusters.

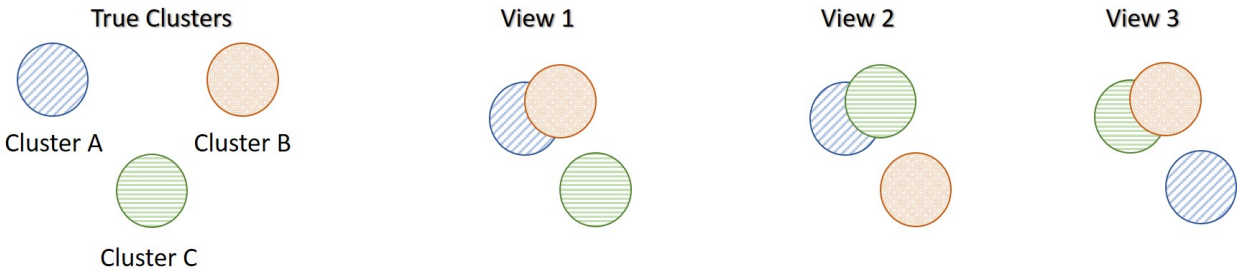


Figure 1: **Data structure of toy example.** Each data-view captures different characteristics of the three clusters, and thus produces different clustering.

2.3 Multi-SNE

SNE Hinton and Roweis [2003] measures the probability distribution (P) of each data point (\mathbf{x}_i) by looking at the similarities among its neighbours. For every sample i in the data, j is taken as its potential neighbour with probability p_{ij} , given by:

$$p_{ij} = \frac{\exp(-d_{ij}^2)}{\sum_{k \neq i} \exp(-d_{ik}^2)}$$

where $d_{ij} = \frac{\|\mathbf{x}_i - \mathbf{x}_j\|^2}{2\sigma_i^2}$ represents the dissimilarity between points \mathbf{x}_i and \mathbf{x}_j . The value of σ_i is either set by hand or found by binary search. The obtained probability distribution $P_i = \sum_j p_{ij}$ has a fixed perplexity, which refers to the effective number of local neighbours. Perplexity is defined as $Perp(P_i) = 2^{H(P_i)}$, where $H(P_i) = -\sum_j p_{ij} \log_2 p_{ij}$ is the Shannon entropy of P_i . It increases monotonically with the variance σ_i and typically takes values between 5 and 50.

By the same token, a probability distribution in the low-dimensional space is computed as follows:

$$q_{ij} = \frac{\exp(-\|\mathbf{y}_i - \mathbf{y}_j\|^2)}{\sum_{k \neq i} \exp(-\|\mathbf{y}_i - \mathbf{y}_k\|^2)}$$

which represents the probability of point i selecting point j as its neighbour.

The induced embedding output (\mathbf{y}_i), represented by probability distribution, Q , is obtained by minimising the Kullback-Leibler divergence (KL-divergence) between the two distributions ($KL(P||Q)$) Kullback and Leibler [1951]. In other words, the cost function to minimise is given as:

$$C_{SNE} = \sum_i KL(P_i||Q_i) = \sum_i \sum_j p_{ij} \log \frac{p_{ij}}{q_{ij}}$$

Gaussian distribution is assumed in computing the similarity between two points in both high and low dimensional spaces. van der Maaten and Hinton [2008] proposed a variant of SNE, called t-SNE, which uses a symmetric version of SNE and a Student t-distribution to compute the similarity between two points in the low-dimensional space (Q), given by:

$$q_{ij} = \frac{(1 + \|\mathbf{y}_i - \mathbf{y}_j\|^2)^{-1}}{\sum_{k \neq i} (1 + \|\mathbf{y}_i - \mathbf{y}_k\|^2)^{-1}}$$

T-SNE is often preferred, because it reduces the effect of crowding problem (limited area to accommodate all data points and differentiate clusters) and it is easier to optimise, as it provides simpler gradients than SNE.

Xie et al. [2011] proposed m-SNE, an extension of t-SNE that integrates multi-view data into a unified induced embedding. The integration is achieved by combining the probability distributions of all different data-views into a single distribution on the high-dimensional space. Thus the probability distribution on the high-dimensional space would be $p_{ij} = \sum_{m=1}^M \beta^m p_{ij}^m$, where β^m is the combination coefficient of the m^{th} data-view, acting as a weight vector and satisfies $\sum_m \beta^m = 1$. The probability distribution under the m^{th} data-view, between data points i and j is represented by p_{ij}^m . This leads to the following cost function:

$$C_{m-SNE} = \sum_i \sum_j \left(\sum_m \beta^m p_{ij}^m \right) \log \frac{\sum_m \beta^m p_{ij}^m}{q_{ij}}$$

We propose a new multi-view extension based on t-SNE, that we call *multi-SNE*. Our proposal is to take the KL-divergence between the distribution of a single induced embedding and each data-view of the data separately, and minimise their weighted sum. While Xie et al. [2011] apply t-SNE on a weighted combination of the probability distribution of all data-views, we propose an iterative algorithm where at each iteration, the induced embedding is updated by minimising the following cost function:

$$C_{multi-SNE} = \sum_m \sum_i \sum_j w^m p_{ij}^m \log \frac{p_{ij}^m}{q_{ij}}$$

In multi-SNE, we seek to avoid combining the probability distributions of all data-views together. Multi-SNE updates the induced embedding by minimising the KL-divergence between every data-view's probability distribution and that of

the low-dimensional representation we seek to obtain. In other words, this is achieved by computing and summing together the gradient descent for each data-view. The induced embedding is then updated by minimising the summed gradient descent. In this study, we have taken equal weights on all data-views, *i.e.* $w^m = \frac{1}{M}$, $\forall m = 1, \dots, M$. Please refer to the Appendix for the algorithm of multi-SNE (Algorithm 1).

T-SNE applied on each single data-view separately captures the correct underlying structure of the data in the toy example (Figure 2). M-SNE improves significantly the visualisation, while multi-SNE separates the three clusters perfectly. T-SNE on concatenated features ($\text{SNE}_{\text{concat}}$) captures mostly the structure of the third data-view, because that data-view has a higher variability between the clusters than the other two. Even with different data structure within each data-view, multi-SNE has the capability of separating clearly the three true clusters by capturing the overall structure of multi-view data.

2.4 Multi-LLE

LLE attempts to discover a non-linear structure of high-dimensional data (X) by computing low-dimensional and neighbourhood-preserving embeddings (Y) Saul and Roweis [2001]. The algorithm performs three steps.

1. Finds a set, denoted by Γ_i , which contains the K nearest neighbours of each data point X_i , $i = 1, \dots, N$, as measured by Euclidean distance. The parameter K is given as input. Other local metrics can also be used in identifying the nearest neighbours.
2. Computes a weight matrix W , which reconstructs X , by minimising the following cost function:

$$\mathcal{E}_X = \sum_i |X_i - \sum_j W_{ij} X_j|^2 \quad (1)$$

where the weights W_{ij} describe the contribution of the j^{th} data point to the i^{th} reconstruction. The optimal weights W_{ij} are found by solving a least squares problem subject to two constraints:

- $W_{ij} = 0$, if $j \notin \Gamma_i$
- $\sum_j W_{ij} = 1$

3. Computes the low-dimensional Y_i of each data point $i = 1, \dots, N$, by minimising:

$$\mathcal{E}_Y = \sum_i |Y_i - \sum_j W_{ij} Y_j|^2 \quad (2)$$

The solution to equation (2), is obtained by taking the bottom d non-zero eigenvectors of a sparse $N \times N$ matrix defined by $M = (I - W)^T(I - W)$.

We explored three separate approaches that would allow the implementation of LLE on multi-view data.

- A. **LLE_{concat}**: Apply LLE on the concatenated features of all data-views.
- B. **m-LLE** - Combine the LLE embeddings of each data-view: Compute the low-dimensional embedding as a weighted average of the embeddings obtained by applying LLE on each data-view separately, *i.e.* computing the weight matrices W^m and solving $\mathcal{E}_{Y^m} = \sum_i |Y_i^m - \sum_j W_{ij}^m Y_j^m|^2$, for each $m = 1, \dots, M$ separately. Thus, the low-dimensional embedding \hat{Y} is obtained by setting $\hat{Y} = \sum_m \beta^m Y^m$, where $\sum_m \beta^m = 1$.
- C. **multi-LLE** - Combine the weight matrices obtained from each data-view: Compute the low-dimensional embedding by using a consensus weight matrix, given by $\hat{W} = \sum_m \alpha^m W^m$, where $\sum_m \alpha^m = 1$, after obtaining the weight matrices W^m for each $m = 1, \dots, M$. Thus, \hat{Y} is obtained by solving $\mathcal{E}_{\hat{Y}} = \sum_i |\hat{Y}_i - \sum_j \hat{W}_{ij} \hat{Y}_j|^2$.

The algorithms of m-LLE and multi-LLE can be found in the Appendix.

On the toy example, multi-LLE produced the best results, as it separated the three true clusters, while the other algorithms did not (Figure 2). Similarly with t-SNE, single-view LLE was able to capture the true underlying structure of each data-view separately, but it failed when we concatenated the features. In particular, $\text{LLE}_{\text{concat}}$ produced an almost identical visualisation with LLE applied on the third data-view, while m-LLE bundles all clusters into one. Based on this example, multi-LLE is the most promising LLE-based multi-view algorithm.

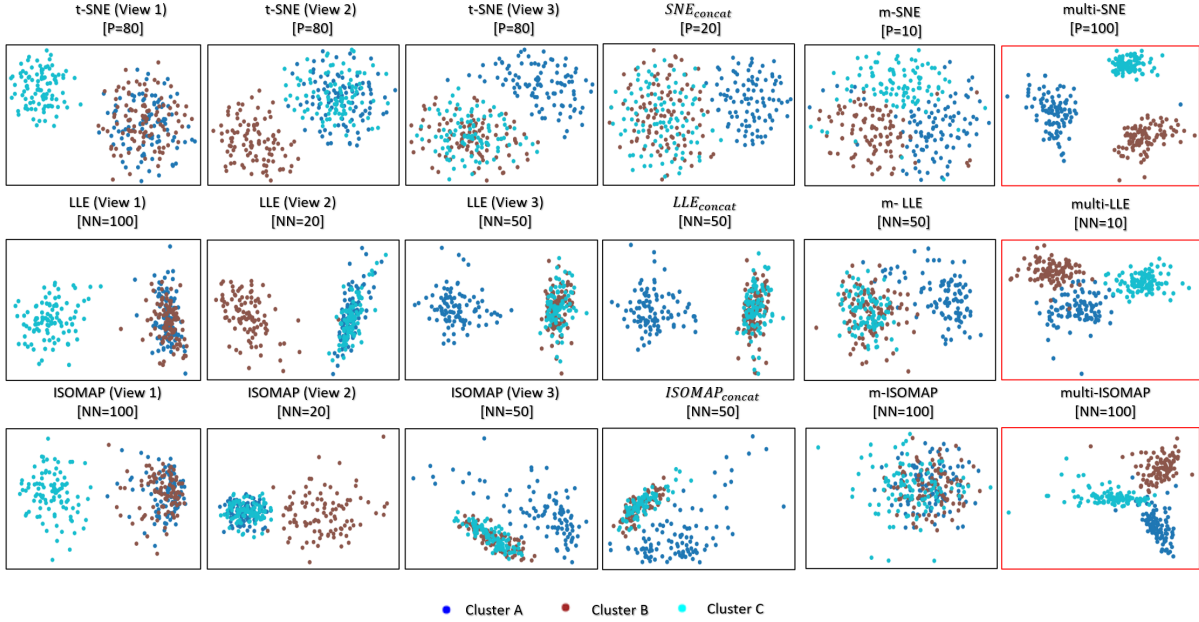


Figure 2: **Visualisations of toy example.** Produced by SNE, LLE, ISOMAP based algorithms. The projections with red frame depict our proposed methods.

2.5 Multi-ISOMAP

ISOMAP aims to discover a low-dimensional embedding of high-dimensional data by maintaining the geodesic distances between all points Tenenbaum et al. [2000]; it is often viewed as an extension of Multi-dimensional Scaling. The ISOMAP algorithm comprises of three steps:

1. Let $G \sim (V, E)$ define a neighbourhood graph, with vertices V representing all data points and the edge length between any two vertices $i, j \in V$ given by a distance metric $d_X(i, j)$. If a vertex j does not belong to the K nearest neighbours of i , then $d_X(i, j) = 0$. The parameter K is given as input.
2. Computes the shortest paths between all pairs of points in G . The shortest path between vertices $i, j \in V$ is defined by $d_G(i, j)$. The most efficient known algorithm to perform this task is Dijkstra’s Algorithm. Alternatively, we can initialize $d_G(i, j) = d_X(i, j)$ and replace all entries by $d_G(i, j) = \min \{d_G(i, k), d_G(k, j)\}$. Let $D_G \in \mathbb{R}^{|V| \times |V|}$ be a matrix containing the shortest paths between any vertices $i, j \in V$, defined by $(D_G)_{ij} = d_G(i, j)$.
3. Constructs the low-dimensional embedding. Let λ_p be the p^{th} eigenvalue in decreasing order of the matrix D_G and u_p^i the i^{th} component of p^{th} eigenvector. Then i^{th} component of the low-dimensional embedding is given by $y_i = \sqrt{\lambda_p} u_p^i$.

We propose a modification which allows the implementation of ISOMAP on multi-view data, called **multi-ISOMAP**. Let $G_m \sim (V, E_m)$ be a neighbourhood graph obtained from data-view $X^{(v)}$ as defined in the first step of ISOMAP. All neighbourhood graphs are then combined into a single graph, \tilde{G} ; the combination is achieved by computing the edge length as the averaged distance of each data-view, i.e. $d_{\tilde{G}}(i, j) = w_m \sum_m d_{G_m}(i, j)$. Once a combined neighbourhood graph is computed, multi-ISOMAP follows steps 2 and 3 of ISOMAP. Throughout this paper we set $w_m = \frac{1}{M}, \forall m$.

Similarly with LLE, we explored and compared multi-ISOMAP with two more trivial extensions of ISOMAP:

- A. **ISOMAP_{concat}**: Apply ISOMAP on the concatenated features of all data-views.
- B. **m-ISOMAP** - Combine the ISOMAP embeddings of each data-view: Compute the overall low-dimensional embedding as a weighted average of the embeddings obtained by applying ISOMAP on each data-view separately, i.e. low-dimensional embedding \hat{Y} is obtained by computing $\hat{Y} = \sum_m \beta^m Y^m$, where $\sum_m \beta^m = 1$.

The true underlying structure of each data-view on the toy example is correctly identified by applying single-view ISOMAP (Figure 2). ISOMAP_{concat} and m-ISOMAP capture the data structure of the third view, as LLE_{concat} and SNE_{concat} did. Multi-ISOMAP separates the three true clusters, but it does not provide a better visualisation than multi-SNE.

Based on the toy example, multi-SNE has shown the most promising results out of all single-view and multi-view manifold learning algorithms considered in this section. SNE, LLE and ISOMAP depend on parameters that their proper tuning ensues to optimal results. The choice of the parameter can influence the visualisations and in some cases present the data into separate maps van der Maaten and Hinton [2012]. For SNE, perplexity is the parameter to tune, while for LLE and ISOMAP, it is the number of nearest neighbours. The same parameters exist in their multi-view extensions presented in this manuscript. The projections presented in Figure 2 are taken after optimising the tuning parameter of each algorithm.

3 Results

This section evaluates the performance of multi-view manifold learning algorithms through simulation studies and real data analyses. We organize this section as follows: In Section 3.1 we present the simulated and real data sets, and their characteristics. In Section 3.2, we show how these algorithms can be used to separate data points into clusters, if they exist. *Handwritten digits* and *caltech7* data sets allow for data clustering and were used for this experiment. In Section 3.3, we conduct two simulation studies to explore the effects of tuning parameters on the multi-view manifold learning algorithms. In Section 3.4, we investigate the optimal number of data-views and the applicability of the algorithms on high-dimensional data. The *cancer types* data set was used to perform this experiment.

We tested the multi-view manifold learning algorithms on real and simulated data-sets for which the true labels are known and we used the truth to tune the parameters. The results presented in this section are after finding the optimal tuning parameters. To do so, we implemented the following procedure: Assume that the data points belong to a number of clusters and we seek to identify them. We explored the performance of the algorithms in a range of tuning parameter values, $S = \{2, 10, 20, 50, 80, 100, 200\}$. The number of nearest neighbours, the parameter in LLE and ISOMAP, cannot exceed the total number of samples in the data. We applied K-means on the low-dimensional embeddings and evaluated the produced clusters against the truth via common clustering measures. If the truth is unknown, manual evaluation of the resulting visualisations can be performed instead.

3.1 Data Description

Data Description		Views	Clusters	Features	Samples	Hetero-	High
	Data Set	(M)	(k)	(size)	(size)	geneous	dimensional
Real	Handwritten Digits	6	10	~ 200	~ 2000	✓	✗
	Caltech7	6	7	~ 1000	~ 1000	✓	✗
	Cancer Types	3	3	> 10000	~ 300	✓	✓
Simulated	Toy Example	3	3	300	300	✗	✗
	NDS	4	3	400	300	✗	✓
	MCS	3	5	300	500	✗	✗

Table 1: **Data summary.** Description of real and simulated data sets.

The real and simulated data sets analysed in this paper are described below:

Handwritten Digits²: Consists of features on handwritten numerals (0 – 9) extracted from a collection of Dutch utility maps. 200 patterns per class (for a total of 2000 patterns) have been digitised in binary images. These digits are represented in terms of six data-views: (a) Fourier coefficients of the character shapes (76 features), (b) profile correlations (216), (c) Karhunen-Love coefficients (64), (d) pixel averages in 2 x 3 windows (240), (e) Zernike moments (47) and (f) morphological features (6) Dua and Graff [2017].

Caltech7³: Caltech-101 contains pictures of objects belonging to 101 categories. This subset of Caltech-101 contains only 7 classes and it was created because of the imbalanced number of objects in each class of Caltech-101. It consists of 1474 objects on six data-views: (a) Gabor (48 features), (b) wavelet moments (40), (c) CENTRIST (254), (d) histogram of oriented gradients (1984), (e) GIST (512), and (f) local binary patterns (928) Fei-Fei et al. [2006].

²<https://archive.ics.uci.edu/ml/datasets/Multiple+Features>

³<https://github.com/yeqinglee/mvdata>

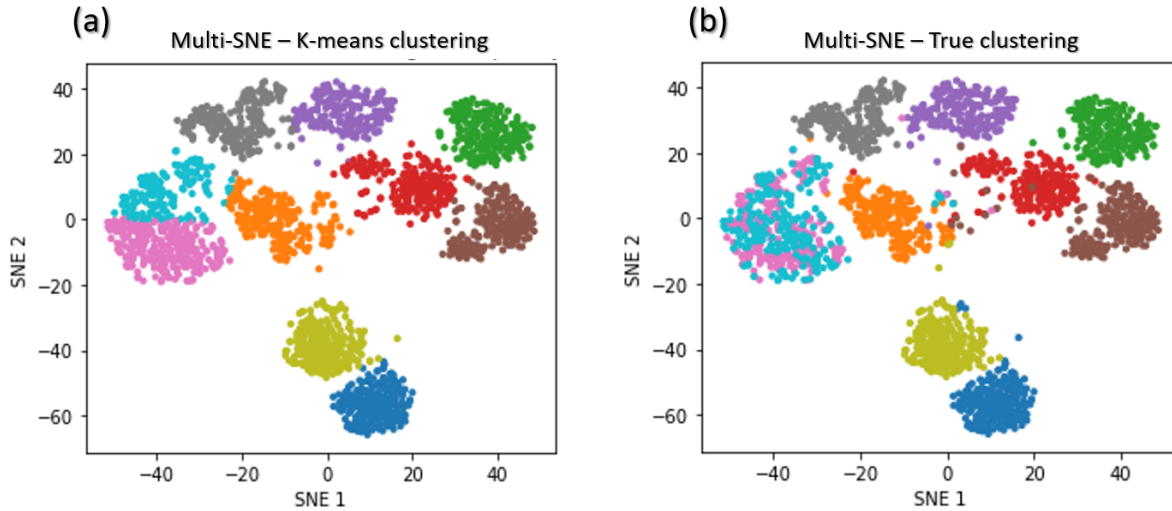


Figure 3: **Visualisations of handwritten digits.** Produced by multi-SNE with perplexity $P = 10$. Colours present the clustering on the data points by (a) K-means, and (b) Truth.

Cancer Types⁴: Consists of 65 patients with breast cancer, 82 with kidney cancer and 106 with lung cancer. This data set consists of three data-views: (a) genomics (10299 genes), (b) epigenomics (22503 methylation sites) and (c) transcriptomics (302 mi-RNA sequences). The aim is to cluster patients by their cancer type Wang et al. [2014].

Noisy Data-view Scenario (NDS): A simulated data set, which consists of 4 data-views and 3 true underlying clusters. The first three data-views follow the same structure as in the toy example, while the 4th data-view represents a completely noisy data-view, *i.e.* all data points lie in a single cluster. $p_v = 100, \forall v, n = 300$, equally balanced data samples.

More Clusters than data-views Scenario (MCS): A simulated data set, which consists of 3 data-views and 5 true underlying clusters. The true underlying structure of the each data-view is shown in Figure 5. $p_v = 100, \forall v, n = 500$, equally balanced data samples.

The different characteristics of each data set used in this study are summarised in Table 1. Their variation in heterogeneity, high-dimensionality, and number of data-views, clusters, features and samples allows us to evaluate the methods in a range of situations we might come across with real and noisy data. Such evaluations are important for choosing the most appropriate method according to the characteristics of the data at hand. We classified the real data sets as heterogeneous due to the nature of their data. The simulated data sets are classified as non-heterogeneous, since they were generated under the same conditions and distributions.

In the simulation studies, we want to explore how the algorithms behave when the separation between the clusters exists, but it is not as explicit as in the toy example. NDS adds a noisy data-view and in MCS we increased the number of clusters, but not the number of data-views.

Handwritten digits data set is characterised by the perfectly balanced data points; each of the ten clusters contains 200 samples. On the other hand, caltech7 is imbalanced with the first two clusters containing much more samples than the rest. The number of samples in each cluster is as follows {A: 435, B: 798, C: 52, D: 34, E: 35, F: 64, G: 56}. We took a random sample of size 50 for clusters A and B in order to create a balanced subset of the caltech7 data set.

3.2 Multi-view Manifold Learning for Clustering

Quantifying the performance of data visualisation algorithms is not trivial. Effective data visualisation can be defined differently according to the visualisation design and the primary reason of visualising the data Zhu [2007]. Casner [1991] argues the data visualisations can be designed for specific tasks and thus effective visualisations are the ones that improve efficiency.

⁴<http://compbio.cs.toronto.edu/SNF/SNF/Software.html>

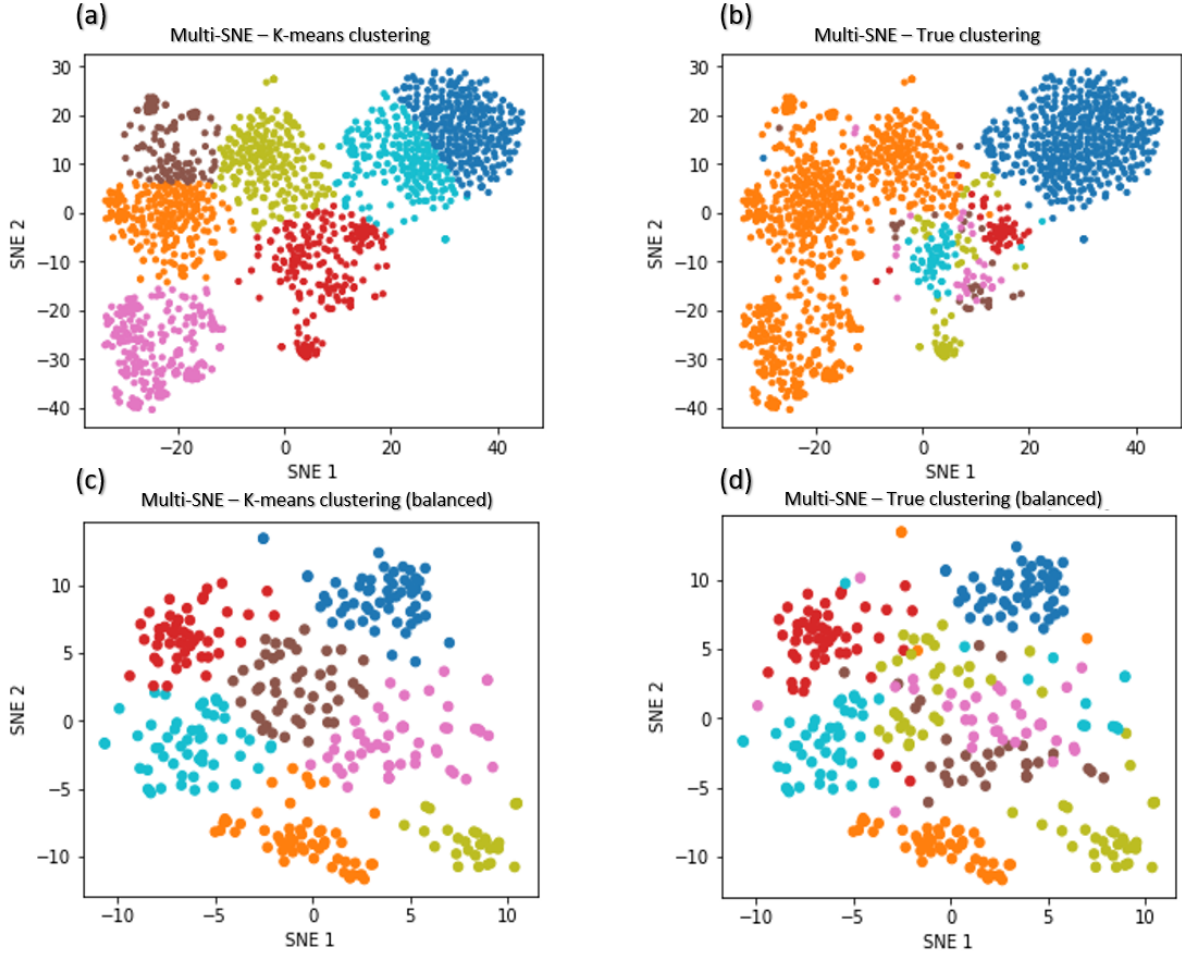


Figure 4: **Visualisations of caltech7 and its balanced subset.** Produced by multi-SNE with perplexity $P = 80$ and $P = 10$ for the original and balanced caltech7, respectively. Colours present the clustering on the data points by (a) and (c) K-means, and (b) and (d) Truth. (a) and (b) present the data points on the entire data set, while (c) and (d) are on a balanced subset.

The purpose of visualisation in this study is to identify patterns within data, and in particular separate data points according to some clusters. Hence, we can evaluate the performance of these methods by performing a clustering analysis on the low-dimensional embeddings obtained by each algorithm. If the two-dimensional embeddings can separate the data points to their respective clusters accurately via a clustering algorithm, then those clusters should be visually well-shown and separated in two dimensions.

In this section, we will quantify the performance of data visualisation algorithms by using two real data sets, namely *handwritten digits* and *caltech7* (and its balanced version). We implemented K-means to cluster the data points for three reasons: (a) it is one of the most prominent and robust clustering algorithms, (b) the number of clusters (k) can be specified and (c) different clusters are separated by the means of their centroids, and thus a better performance of K-means would suggest a visually clearer separation of clusters.

Given that the truth (actual clusters of the data) is known, four evaluation measures, commonly used in data clustering, were computed: (i) Accuracy (ACC), (ii) Normalised Mutual Information (NMI) Vinh et al. [2010], (iii) Rand Index (RI) Rand [1971] and (iv) Adjusted Rand Index (ARI) Hubert and Arabie [1985]. All measures can take values in the range $[0, 1]$, with 0 expressing complete randomness, and 1 perfect separation between clusters. The mathematical formulas of the four measures are described in the Appendix.

Implementing K-means on the low-dimensional embedding of multi-SNE applied on handwritten digits produces results directly comparable with the truth (Figure 3). The clusters reflecting the digits 6 and 9 are clustered together, but all

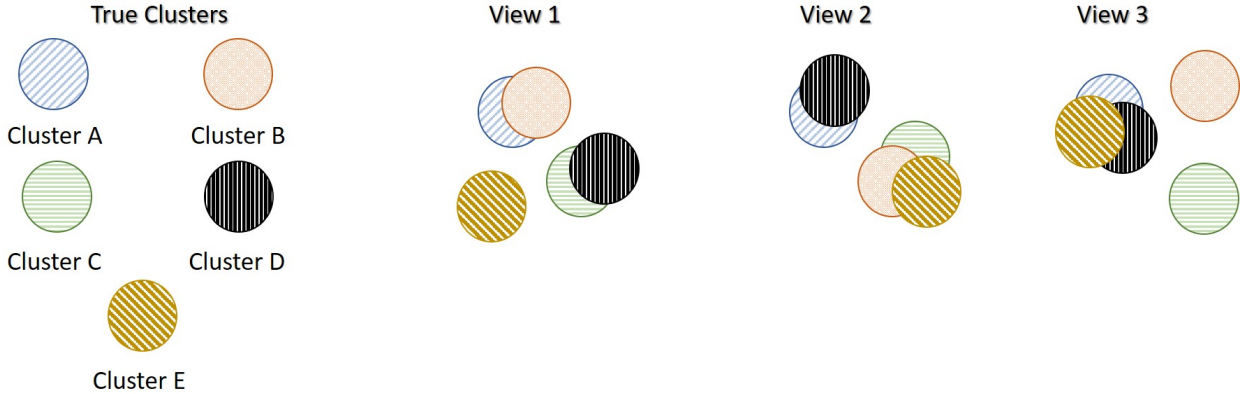


Figure 5: **Data structure of MCS.** Each data-view captures different characteristics of the five clusters, and thus produces different clusterings.

remaining clusters are well separated and agree with the truth. Thus, in this case it would be sensible to evaluate the method’s performance via the measures mentioned above. However, this is not the case for the caltech7 data set.

Multi-SNE applied on caltech7 produces a good visualisation, with clusters A and B being clearly separated from the rest (Figure 4b). Clusters C and G are also well-separated, but the remaining three clusters are bundled together. Applying K-means to that low-dimensional embedding does not capture the true clusters. K-means provides a solution for which the clusters are equally sized (Figure 4a). Hence, quantifying the performance of multi-SNE based on the K-means clustering in this example would provide misleading results, as Table 2 shows.

Data visualisation of the balanced subset of caltech7 with K-means and true clustering are presented in Figures 4c and 4d, respectively. Similarly to Figure 4b, clusters A, B, C and G are well-separated, while the remaining are still bundled together. By using a well-balanced subset of the data set, we make the same conclusions in terms of pattern recognition with the advantage of having comparable clusterings with the truth. Thus evaluating the multi-view algorithms on this subset would be more sensible and less misleading.

Multi-SNE had a superior performance among all algorithms on all measures for both handwritten digits and balanced caltech7 data sets (Table 2). Multi-LLE and multi-ISOMAP were the best among LLE and ISOMAP based algorithms, respectively.

Concluding, in pattern recognition tasks, this study shows that evaluating data visualisation via clustering analyses can be a sensible choice, as long as the data are well-balanced.

3.3 Optimal Parameter Selection

SNE, LLE and ISOMAP depend on an optimization parameter. Even though the parameter is defined differently in each algorithm, it is always related to the nearest global neighbours. As previously discussed, the optimal parameter is found by comparing the performance of the methods on the range $S = \{2, 10, 20, 50, 80, 100, 200\}$.

To find the optimal parameter value, we evaluated the performance of the algorithms by applying K-means on the low-dimensional embeddings and comparing the resulting clusterings against the truth. Once the optimal parameter was found, we confirmed that the clusters were visually separated by manually looking at the two-dimensional embeddings. Since the data are perfectly balanced and were generated for clustering, this approach can effectively evaluate the data visualisations.

Single-view SNE, LLE and ISOMAP algorithms produced a misclustering error of 0.3, meaning that a third of the samples was incorrectly clustered (in this case cluster C). This shows that single-view methods capture the true underlying structure of each simulated data-view (Figure 7b). The only exception for NDS is the fourth data-view, for which the error is closer to 0.6, *i.e.* randomly assigns the clusters (follows the simulation design). After concatenating the features of all data-views, the performance remains poor (Figure 7a). The variance of the misclustering error on this solution is much greater, suggesting that single-view manifold learning algorithms on concatenated data are not robust and thus not reliable.

Data Set	Algorithm	Accuracy	NMI	RI	ARI
Handwritten Digits	SNE _{concat} [P=10]	0.714	0.731	0.932	0.635
	m-SNE [P=10]	0.746	0.741	0.930	0.638
	multi-SNE [P=10]	0.822	0.863	0.963	0.802
	LLE _{concat} [NN=10]	0.562	0.560	0.871	0.441
	m-LLE [NN=10]	0.632	0.612	0.896	0.503
	multi-LLE [NN=5]	0.614	0.645	0.897	0.524
	ISOMAP _{concat} [NN=20]	0.634	0.619	0.905	0.502
	m-ISOMAP [NN=20]	0.636	0.628	0.898	0.477
	multi-ISOMAP [NN=5]	0.658	0.631	0.909	0.518
Caltech7	SNE _{concat} [P=50]	0.398	0.311	0.676	0.226
	m-SNE [P=10]	0.559	0.534	0.766	0.457
	multi-SNE [P=80]	0.541	0.472	0.726	0.350
	LLE _{concat} [NN=100]	0.434	0.283	0.792	0.188
	m-LLE [NN=5]	0.431	0.313	0.767	0.221
	multi-LLE [NN=80]	0.513	0.380	0.788	0.264
	ISOMAP _{concat} [NN=20]	0.388	0.295	0.678	0.247
	m-ISOMAP [NN=5]	0.416	0.306	0.686	0.261
	multi-ISOMAP [NN=10]	0.521	0.354	0.727	0.367
Caltech7 (balanced)	SNE _{concat} [P=80]	0.474	0.318	0.700	0.293
	m-SNE [P=10]	0.563	0.406	0.829	0.337
	multi-SNE [P=20]	0.762	0.688	0.908	0.631
	LLE _{concat} [NN=20]	0.567	0.348	0.725	0.380
	m-LLE [NN=10]	0.403	0.169	0.617	0.139
	multi-LLE [NN=5]	0.622	0.454	0.71	0.391
	ISOMAP _{concat} [NN=5]	0.434	0.320	0.791	0.208
	m-ISOMAP [NN=5]	0.455	0.299	0.797	0.224
	multi-ISOMAP [NN=5]	0.548	0.368	0.81	0.267
NDS	SNE _{concat} [P=80]	0.747	0.628	0.817	0.598
	m-SNE [P=50]	0.650	0.748	0.766	0.629
	multi-SNE [P=80]	0.989	0.951	0.969	0.987
	LLE _{concat} [NN=5]	0.606	0.477	0.684	0.446
	m-LLE [NN=20]	0.685	0.555	0.768	0.528
	multi-LLE [NN=20]	0.937	0.768	0.922	0.823
	ISOMAP _{concat} [NN=100]	0.649	0.528	0.750	0.475
	m-ISOMAP [NN=5]	0.610	0.453	0.760	0.386
	multi-ISOMAP [NN=300]	0.778	0.788	0.867	0.730
MCS	SNE _{concat} [P=200]	0.421	0.215	0.711	0.173
	m-SNE [P=2]	0.641	0.670	0.854	0.575
	multi-SNE [P=50]	0.919	0.862	0.942	0.819
	LLE _{concat} [NN=50]	0.569	0.533	0.796	0.432
	m-LLE [NN=20]	0.540	0.627	0.819	0.487
	multi-LLE [NN=20]	0.798	0.647	0.872	0.607
	ISOMAP _{concat} [NN=150]	0.628	0.636	0.834	0.526
	m-ISOMAP [NN=5]	0.686	0.660	0.841	0.565
	multi-ISOMAP [NN=300]	0.717	0.630	0.852	0.570

Table 2: **Clustering performance.** For each data set, **red** highlights the method with the best performance on each measure between each group of algorithms (SNE, LLE or ISOMAP based). The overall superior method for each data set is depicted with **bold**. The parameters P and NN refer to the selected perplexity and number of nearest neighbours, respectively. They were optimised for the corresponding methods.

On both NDS and MCS, multi-LLE and multi-SNE rely heavily on their corresponding parameter value (Figures 7a and 6). While multi-SNE provided better results as perplexity was increasing, multi-LLE performed the best when the number of nearest neighbours was low. On the other hand, multi-ISOMAP had the highest NMI value when the parameter was large.

Overall, ISOMAP-based multi-view algorithms showed a higher variability than the other multi-view methods, which makes them less favourable solutions. The performance of ISOMAP-based methods improved as the parameter value increased (Figure 6). However, they were outperformed by multi-LLE and multi-SNE on both simulation studies.

Out of the three manifold learning foundations, LLE-based solutions depend the most on their parameter value to produce the optimal outcome. Their performance dropped when the parameter value lay between 20 and 100 (Figure 7a). When the number of nearest neighbours was set to be greater than 100 their performance started to improve. Out of all LLE-based algorithms, the highest NMI and lowest misclustering error was obtained by multi-LLE (Figures 7 and 6).

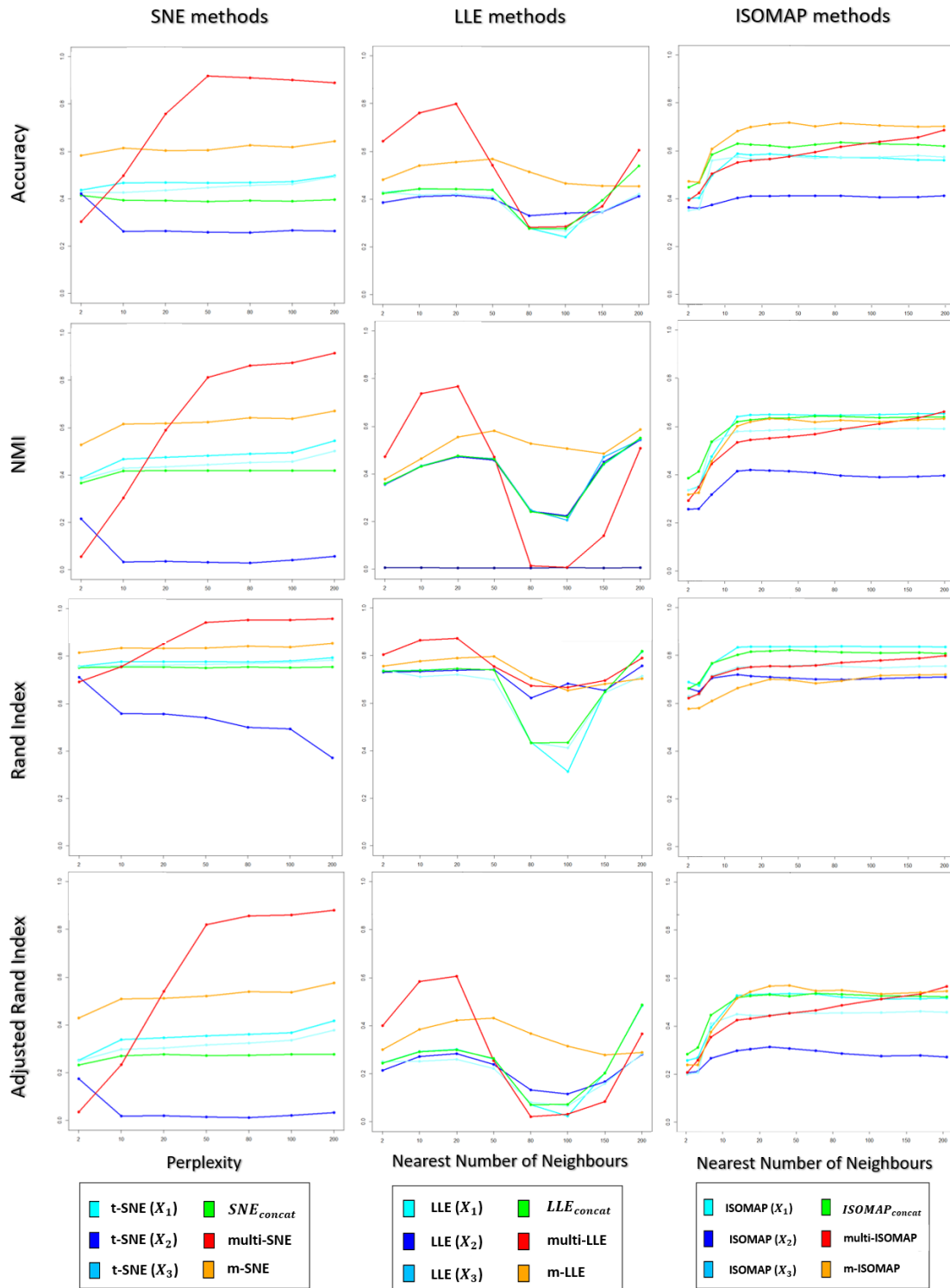


Figure 6: **MCS evaluation measures.** The clustering evaluation measures plotted against different parameter values on the three manifold learning algorithms.

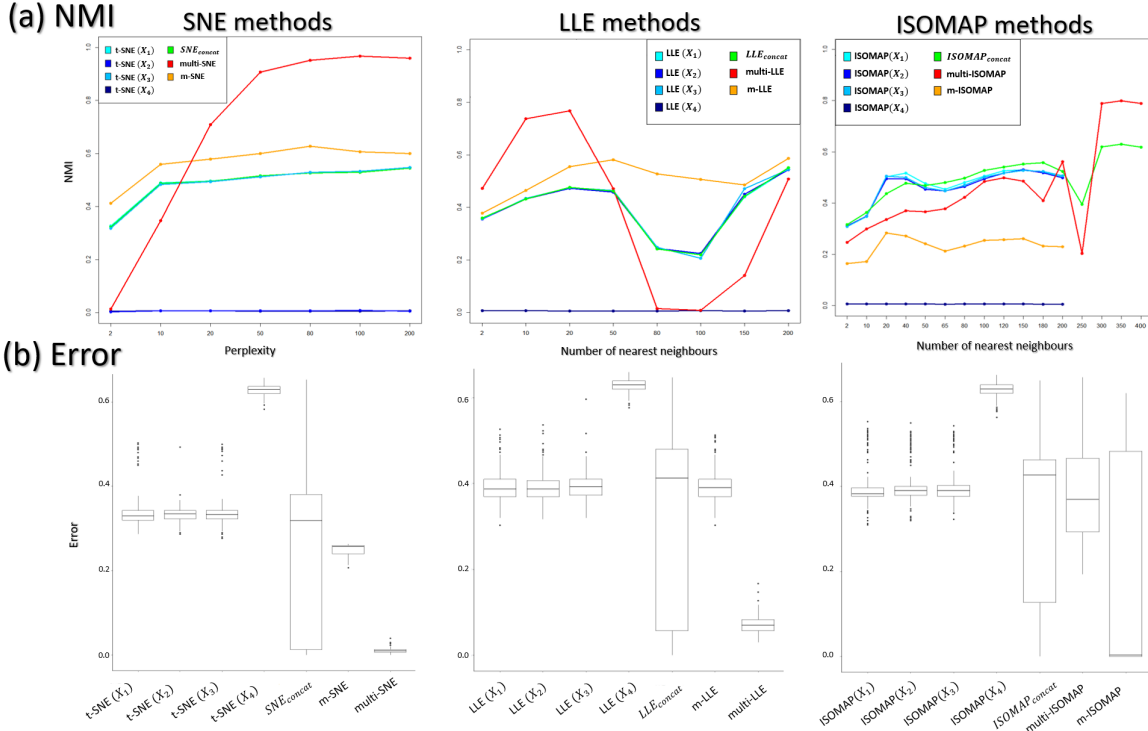


Figure 7: **NDS evaluation measures.** (a) NMI values along different parameter values on all manifold learning algorithms and (b) Error values on the optimal parameter values.

Even though, m-SNE improved the performance of single-view methods in terms of both clustering and error variability, multi-SNE produced the best results (Figures 7 and 6). In particular, multi-SNE outperformed all algorithms presented in this paper on both NDS and MCS. Even though it performed poorly for low perplexity values, its performance improved for $Perp \geq 20$. Multi-SNE was the algorithm with the lowest error variance, making it a robust and preferable solution.

3.4 Optimal Number of Data-views and High-dimensionality

The goal of this section is to determine whether it would be optimal to use all available data-views or discard some possibly noisy data-views. We present here only the outcomes from SNE-based algorithms, as they have shown the most promising results (Table 2).

It is common to think that more information would lead to better results, and in theory that should be the case. However, in practice that is not always true Kumar et al. [2011]. Cancer types data set, which consists of three data-views (genomics, epigenomics and transcriptomics) on the same patients has been used to explore this hypothesis. With three available data-views, we implemented a multi-view visualisation on three combinations of two data-views and a single combination of three data-views.

The genomics data-view provides a reasonably good separation of the three cancer types, whereas miRNA data-view fails in this task and provides a visualisation that reflects random noise (Figure 8). Concatenating features from the different data-views before implementing t-SNE does not improve the final outcome of the algorithm, regardless of the data-view combination.

Overall, multi-view manifold learning algorithms have improved the data visualisation to a great extent. When all three data-views are considered, both algorithms provide a good separation of the clusters (Figure 8). However, the true cancer types can be identified perfectly when the miRNA data-view is discarded. In other words, the optimal solution in this data set is obtained when only genomics and epigenomics data-views are used. That is because miRNA data-view contains little information about the cancer types and adds random noise, which makes the task of separating the data points more difficult.

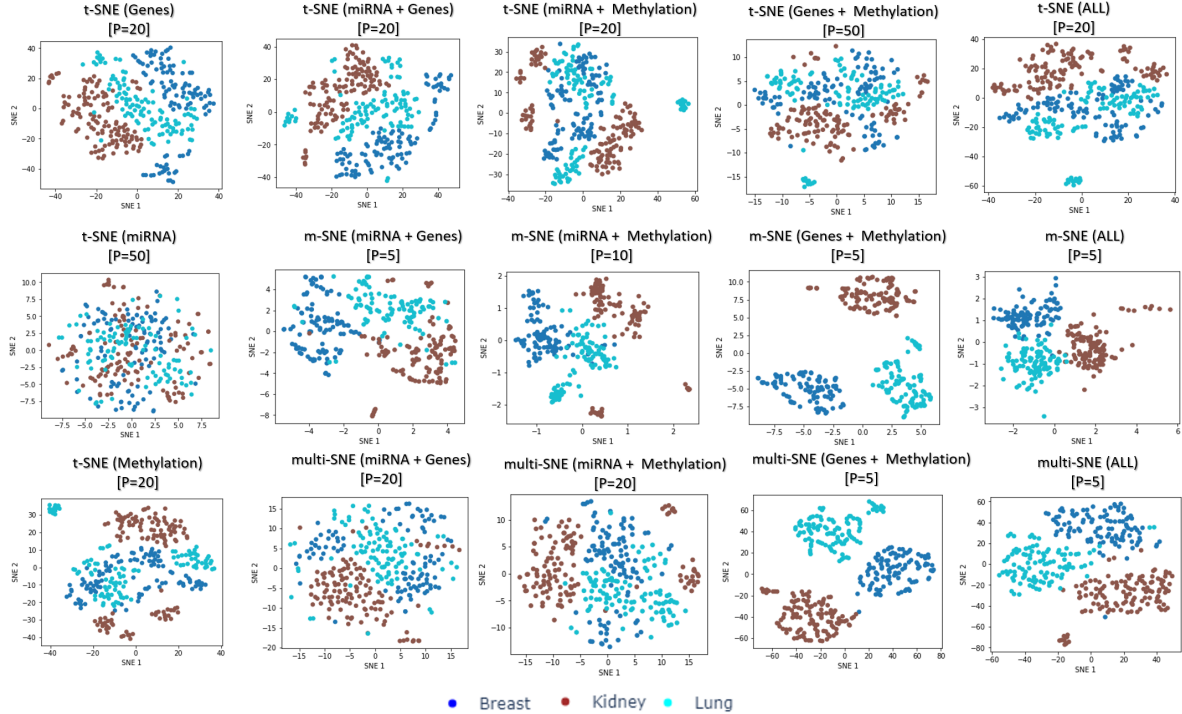


Figure 8: **Visualisations of cancer types.** Produced by all SNE-based manifold learning algorithms on all possible combinations between the three data-views in cancer types data set.

Through the conducted analysis in this section, we have reached two important conclusions: (A) It is not always a good idea to include all available data-views in multi-view manifold learning algorithms; some data-views may provide noise which would result in a worse visualisation than discarding those data-views entirely. The noise of a data-view with unknown labels may be viewed in a single-view t-SNE plot (all data-points in a single cluster), or identified, if possible, via quantification measures such as signal-to-noise ratio. (B) Multi-view manifold learning algorithms can be effectively applied on heterogeneous and high-dimensional data (*i.e.* $p \gg n$).

4 Discussion

The increasing number of multi-view, high-dimensional and heterogeneous data calls for visualisation techniques that would produce an expressive and revealing depiction of such data. In this paper, we propose multi-SNE, a new approach for visualising multi-view data. It is similar to m-SNE, and the different cost functions of the two methods result into two separate, but directly comparable solutions. In addition, we proposed multi-LLE and multi-ISOMAP, which are multi-view manifold learning solutions based on LLE and ISOMAP, respectively.

By investigating simulated and real multi-view data sets, each with different data characteristics, we conclude that multi-SNE provides a more accurate and robust solution than other single-view and multi-view manifold learning algorithms. Specifically, multi-SNE was able to produce the best data visualisations of all data sets analysed in this paper. Multi-LLE provides the second best solution, while multi-view ISOMAP algorithms have not produced great visualisations.

To evaluate these algorithms we quantified the low-dimensional embeddings by finding clusters in the data and comparing them to the truth. We followed this approach to determine the optimal parameter value for each algorithm. We concluded that SNE-based methods perform the best when perplexity is in the range $[20, 100]$, for LLE-based the number of nearest neighbours should be small, in the range $[10, 50]$, while ISOMAP-based methods should take large values, in the range $[100, N]$, where N is the number of samples.

This evaluation process assumes that the data allow for clustering. The handwritten digits data set is a popular multi-view data set for this task. It has been used in multiple studies to illustrate the performance of multi-view clustering

Multi-view Clustering on handwritten digits data set									
	Kumar et al. (2011)	Liu et al. (2013)	Sun et al. (2015)	Ou et al. (2016)	Ou et al. (2018)	2D	multi-SNE		
							3D	5D	10D
NMI	0.768	0.804	0.876	0.785	0.804	0.863	0.894	0.897	0.899
ACC	–	0.881	–	0.876	0.880	0.822	0.848	0.854	0.849

Table 3: **Multi-view clustering performance on handwrittend digits.** NMI and Accuracy (ACC) values as they were presented by the authors in their corresponding papers.

Running time	Toy Example	NDS	MCS	Caltech7	Handwritten Digits	Cancer Types
m-SNE	0.43 (0.019)	0.29 (0.07)	0.42 (0.01)	4.29 (0.54)	13.34 (3.43)	251.71 (15.68)
multi-SNE	1.07 (0.100)	0.78 (0.14)	1.02 (0.01)	15.95 (0.71)	45.76 (8.44)	252.00 (11.23)
m-LLE	0.25 (0.071)	0.40 (0.12)	0.42 (0.34)	37.5 (2.21)	26.28 (8.82)	159.52 (17.49)
multi-LLE	0.28 (0.099)	0.41 (0.15)	0.30 (0.14)	37.9 (2.57)	27.94 (5.29)	157.73 (18.19)
m-ISOMAP	0.22 (0.015)	0.57 (0.06)	0.37 (0.01)	38.07 (3.09)	29.52 (5.37)	154.83 (18.04)
multi-ISOMAP	0.24 (0.032)	0.54 (0.13)	0.33 (0.05)	21.23 (2.24)	16.77 (4.65)	85.47 (14.57)

Table 4: **Averaged running time recorded in minutes.** Taken for each manifold learning algorithm on all data sets seen in this paper; standard deviation is given in the parentheses. All algorithms ran on High Performance Computing with 4 nodes.

algorithms, such as those proposed by Kumar et al. [2011], Liu et al. [2013], Sun et al. [2015], Ou et al. [2016] and Ou et al. [2018]. By looking at the NMI values as they were given in their corresponding articles, we conclude that the performance of multi-SNE with K-means is comparable to the best performance of such algorithms (Table 3). Thus, by applying K-means to the low-dimensional embeddings, multi-SNE can successfully tackle multi-view clustering.

Motivated by this result, we repeated this process on a three-dimensional embedding obtained by multi-SNE. By doing so, the clustering performance on handwritten digits was improved (Table 3), with NMI exceeding the results of other multi-view clustering algorithms that experimented with this data set in their studies. However, increasing the dimensions to 5 or 10 latent embeddings, did not have any further effect on the clustering performance (Table 3). We conclude that for the handwritten digits data set, reducing the dimensions to 3 latent embeddings via multi-SNE produces the best visualisation and clustering results (see Appendix for a 3-dimensional visualisation via multi-SNE).

In terms of computational time, none of the multi-view manifold learning algorithms was consistently faster than the rest (Table 4). However, multi-SNE was often the slowest algorithm, while m-SNE and multi-ISOMAP had the fastest computational time.

Further, we demonstrated that in a multi-view setting taking all available data-views does not necessarily produce the best results. By investigating one of the data sets, we recognised that if a data-view contains more noise than signal, it is likely that the visualisation will worsen and thus it would be preferable to discard entirely the noisy data-view. Alternatively, the weight matrices, indicating how much information each data-view contributes to the final embeddings, can be further explored and adjusted for better results.

The lack of multi-view data visualisation techniques, calls for the research and development of such algorithms. These techniques would greatly benefit in gaining a deeper and clearer understanding of such data. In this study, we have introduced several new multi-view manifold learning methods and explored their performance on several data sets. Overall, we find that multi-SNE has great performance in visualisation and clustering of multi-view data.

References

- Stephen M. Casner. Task-analytic approach to the automated design of graphic presentations. *ACM Transactions on Graphics*, 10(2):111–151, 1991.
- Tat-Seng Chua, Jinhui Tang, Richang Hong, Haojie Li, Zhiping Luo, and Yan-Tao Zheng. Nus-wide: A real-world web image database from national university of singapore. In *Proceedings of the 2009 ACM International Conference on Image and Video Retrieval*, 2009.
- Dick de Ridder, Olga Kouropteva, Oleg Okun, Matti Pietikäinen, and Robert P. W. Duin. Supervised locally linear embedding. In *Artificial Neural Networks and Neural Information Processing 2003*, pages 333–341, 2003.
- Dheeru Dua and Casey Graff. UCI machine learning repository, 2017.
- Li Fei-Fei, Rob Fergus, and Perona Pietro. One-shot learning of object categories. *IEEE Transactions on Pattern Analysis and Machine Intelligence*, 28(4):594–611, 2006.
- Yun Fu, Liangliang Cao, Guodong Guo, and Thomas S. Huang. Multiple feature fusion by subspace learning. In *Proceedings of the 2008 International Conference on Content-Based Image and Video Retrieval*, page 127–134, 2008.
- Patrick J.F Groenen and Ingwer Borg. The past, present, and future of multidimensional scaling. Econometric institute research papers, 2013.
- Yehudit Hasin, Marcus Seldin, and Aldons Lusic. Multi-omics approaches to disease. *Genome Biology*, 18, 2017.
- Geoffrey E. Hinton and Sam T. Roweis. Stochastic neighbor embedding. *Advances in Neural Information Processing Systems*, pages 857–864, 2003.
- Lawrence Hubert and Phipps Arabie. Comparing partitions. *Journal of Classification*, 2:193–218, 1985.
- Kanghua Hui and Chunheng Wang. Clustering-based locally linear embedding. In *2008 19th International Conference on Pattern Recognition*, pages 1–4, 2008.
- Solomon Kullback and Richard A. Leibler. On information and sufficiency. 22:79–86, 1951.
- Abhishek Kumar, Piyush Rai, and Daume Hal. Co-regularized multi-view spectral clustering. In *Advances in Neural Information Processing Systems 24*, pages 1413–1421, 2011.
- Gen Li, Xiaokang Liu, and Kun Chen. Integrative multi-view regression: Bridging group-sparse and low-rank models. *Biometrics*, 75:593 – 602, 2019.
- Mingai Li, Xinyong Luo, Jinfu Yang, and Yanjun Sun. Applying a locally linear embedding algorithm for feature extraction and visualization of mi-eeg. *Journal of Sensors*, 2016, 2016.
- Xiangyuan Li, Cheng Cai, and Jinrong He. Density-based multi-manifold isomap for data classification. In *2017 Asia-Pacific Signal and Information Processing Association Annual Summit and Conference (APSIPA ASC)*, pages 897–903, 2017.
- George C. Linderman and Stefan Steinerberger. Clustering with t-sne, provably. *SIAM Journal on Mathematics of Data Science*, 1(2):313–332, 2019.
- Jialu Liu, Chi Wang, Jing Gao, and Jiawei Han. Multi-view clustering via joint nonnegative matrix factorization. *Proceedings of the 2013 SIAM International Conference on Data Mining*, pages 252–260, 2013.
- Leland McInnes, John Healy, Nathaniel Saul, and Lukas Großberger. Umap: Uniform manifold approximation and projection. *Journal of Open Source Software*, 3(29):861, 2018.
- Andrew Y. Ng, Michael I. Jordan, and Yair Weiss. On spectral clustering: analysis and an algorithm. In *Proceedings of the Fourteenth International Conference on Neural Information Processing Systems: Natural and Synthetic*, pages 849–856, 2001.
- Weihua Ou, Shujian Yu, Gai Li, Jian Lu, Kesheng Zhang, and Gang Xie. Multi-view non-negative matrix factorization by patch alignment framework with view consistency. *Neurocomputing*, 204:116 – 124, 2016.
- Weihua Ou, Fei Long, Yi Tan, Shujian Yu, and Wang Pengpeng. Co-regularized multiview nonnegative matrix factorization with correlation constraint for representation learning. *Multimedia Tools and Applications*, 77:12955–12978, 2018.
- William M. Rand. Objective criteria for the evaluation of clustering methods. *Journal of the American Statistical Association*, 66(336):846–850, 1971.
- Theodoulos Rodosthenous and Vahid Shahrezaei and Marina Evangelou Integrating multi-OMICS data through sparse canonical correlation analysis for the prediction of complex traits: a comparison study *Bioinformatics*, 36(17): 4616-4625, 2020.

- Sam T. Roweis and Lawrence K. Saul. Nonlinear dimensionality reduction by locally linear embedding. *Science*, 290: 2323–2326, 2000.
- Lawrence Saul and Sam Roweis. An introduction to locally linear embedding. *Journal of Machine Learning Research*, 7, 01 2001.
- Erich Schubert and Michael Gertz. Intrinsic t-stochastic neighbor embedding for visualization and outlier detection. In *Similarity Search and Applications*, pages 188–203, 2017.
- Hualei Shen, Dacheng Tao, and Dianfu Ma. Multiview locally linear embedding for effective medical image retrieval. *PLOS ONE*, 8(12):1–21, 2013.
- Ting Shu, Bob Zhang, and Yuan Yan Tang. Multi-view classification via a fast and effective multi-view nearest-subspace classifier. *IEEE Access*, 7:49669–49679, 2019.
- Jiangwen Sun, Jin Lu, Tingyang Xu, and Jinbo Bi. Multi-view sparse co-clustering via proximal alternating linearized minimization. volume 37 of *Proceedings of Machine Learning Research*, pages 757–766, 2015.
- Shiliang Sun. A survey of multi-view machine learning. *Neural Computing and Applications*, 23:2031 – 2038, 2013.
- Joshua B. Tenenbaum, Vin de Silva, and John C. Langford. A global geometric framework for nonlinear dimensionality reduction. *Science*, 290:2319–2323, 2000.
- Laurens van der Maaten and Geoffrey Hinton. Visualising data using t-sne. *Journal of Machine Learning Research*, 9: 2579–2605, 2008.
- Laurens van der Maaten and Geoffrey Hinton. Visualizing non-metric similarities in multiple maps. *Machine Learning*, 87(1), 2012.
- Nguyen Xuan Vinh, Julien Epps, and James Bailey. Information theoretic measures for clusterings comparison: Variants, properties, normalization and correction for chance. *Journal of Machine Learning Research*, 11:2837–2854, 2010.
- Bo Wang, Aziz M. Mezlini, Feyyaz Demir, Marc Fiume, Zhuowen Tu, Michael Brudno, Benjamin Haibe-Kains, and Anna Goldenberg. Similarity network fusion for aggregating data types on a genomic scale. *Nature Methods*, 11(3): 333–337, 2014.
- Shiming Xiang, Feiping Nie, Chunhong Pan, and Changshui Zhang. Regression reformulations of l1e and l1sa with locally linear transformation. *IEEE Transactions on Systems, Man, and Cybernetics, Part B (Cybernetics)*, 41(5): 1250–1262, 2011.
- Bo Xie, Yang Mu, Dacheng Tao, and Kaiqi Huang. m-sne: multiview stochastic neighbor embedding. *IEEE Transactions on Systems, Man, and Cybernetics, Part B: Cybernetics*, 41:1088–1096, 2011.
- Chang Xu, Dacheng Tao, and Chao Xu. A survey on multi-view learning. *ArXiv*, abs/1304.5634, 2013.
- Chang Xu, Dacheng Tao, and Chao Xu. Multi-view intact space learning. *IEEE Transactions on Pattern Analysis and Machine Intelligence*, 37(12):2531–2544, 2015.
- Fanghua Ye, Zitai Chen, Hui Qian, Rui Li, Chuan Chen, and Zibin Zheng. New approaches in multi-view clustering. In *Recent Applications in Data Clustering*, chapter 11. 2018.
- Hong Yu, Xianchao Zhang, Yuansheng Yang, Xiaowei Zhao, and Lei Cai. An extended isomap by enhancing similarity for clustering. In *Advanced Research in Applied Artificial Intelligence*, pages 808–815, 2012.
- Zhenyue Zhang and Hongyuan Zha. Principal manifolds and nonlinear dimensionality reduction via tangent space alignment. *SIAM Journal on Scientific Computing*, 8:406–424, 2004.
- Jing Zhao, Xijiong Xie, Xin Xu, and Shiliang Sun. Multi-view learning overview: Recent progress and new challenges. *Information Fusion*, 38:43 – 54, 2017.
- Yue Zhao, Xinge You, Shujian Yu, Chang Xu, Wei Yuan, Xiao-Yuan Jing, Taiping Zhang, and Dacheng Tao. Multi-view manifold learning with locality alignment. *Pattern Recognition*, 78:154 – 166, 2018.
- Nanning Zheng and Jianru Xue. *Manifold Learning*, pages 87–119. 2009.
- Ying Zhu. Measuring effective data visualization. In *Advances in Visual Computing*, pages 652–661, 2007.

A Algorithms

Data: M data sets, $X_m \in \mathbb{R}^{n \times p_m}$, $\forall m \in \{1, \dots, M\}$
Parameters: $Perp$ [Perplexity]; T [Number of iterations]; η [Learning rate]; $\alpha(t)$ [Momentum]
Result: Induced embedding, $Y \in \mathbb{R}^{n \times d}$. Often, $d = 2$
begin
 Compute pairwise affinities $p_{i|j}^m$ with perplexity $Perp$, $\forall m \in \{1, \dots, M\}$
 Set $p_{ij}^m = \frac{p_{i|j}^m + p_{j|i}^m}{2n}$, $\forall m \in \{1, \dots, M\}$
 Initialise solution $Y^{(0)} \sim \mathcal{N}(0, 0.1)$
 for $t=1$ **to** T **do**
 Compute induced affinities $q_{i|j}$ and set sum of gradients, $G = 0$
 for $m=1$ **to** M **do**
 Compute gradient $\frac{\delta C_m}{\delta Y}$
 $G \leftarrow G + \frac{\delta C_m}{\delta Y}$
 end
 Set $Y^{(t)} = Y^{(t-1)} + \eta G + \alpha(t)(Y^{(t-1)} - Y^{(t-2)})$
 end
end

Algorithm 1: Multi-SNE

Data: M data sets, $X_m \in \mathbb{R}^{n \times p_m}$, $\forall m \in \{1, \dots, M\}$
Parameters: k [Number of neighbours]
Result: Induced embedding, $\hat{Y} \in \mathbb{R}^{n \times d}$. Often, $d = 2$
begin
 for $m=1$ **to** M **do**
 Find k nearest neighbours of X^m
 Compute W^m by minimising equation (1)
 Compute the d -dimensional embeddings Y^m by minimising equation (2) under W^m
 end
 Let $\hat{Y} = \sum_m \beta^m Y^m$, where $\sum_m \beta^m = 1$.
end

Algorithm 2: m-LLE

Data: M data sets, $X_m \in \mathbb{R}^{n \times p_m}$, $\forall m \in \{1, \dots, M\}$
Parameters: k [Number of neighbours]
Result: Induced embedding, $\hat{Y} \in \mathbb{R}^{n \times d}$. Often, $d = 2$
begin
 for $m=1$ **to** M **do**
 Find k nearest neighbours of X^m
 Compute W^m by minimising equation (1)
 end
 Let $\hat{W} = \sum_m \alpha^m W^m$, where $\sum_m \alpha^m = 1$.
 Compute the d -dimensional embeddings \hat{Y}^m by minimising equation (2) under \hat{W}
end

Algorithm 3: multi-LLE

B Data Clustering Evaluation Measures

Let $\mathbf{X} = \{X_1, \dots, X_r\}$ be the true classes of the data and $\mathbf{Y} = \{Y_1, \dots, Y_s\}$ the clusterings found on N objects. In this study, we assumed to know the number of clusters and thus set $r = s$. Let n_{ij} be the number of objects in X_i and Y_j . A contingency table is defined as shown in Table 5 below.

	Y_1	Y_2	\dots	Y_s	$\sum_j^s Y_j$
X_1	n_{11}	n_{12}	\dots	n_{1s}	$\sum_i^r n_{1i} = a_1$
X_2	n_{21}	n_{22}	\dots	n_{2s}	a_2
\vdots	\vdots	\ddots	\vdots	\vdots	\vdots
X_r	n_{r1}	n_{r2}	\dots	n_{rs}	a_r
	$\sum_i^r n_{i1} = b_1$	b_2	\dots	b_s	$\mathbf{S} = \sum_i^r \sum_j^s n_{ij}$

Table 5: A contingency table for data clustering. X_i refers to the i^{th} class (truth) and Y_j refers to the j^{th} cluster. n_{ij} are the number of samples found in class i and cluster j . In this study, we take $r = s$, as we performed K-means with the true number of classes known.

The formulas of the four measures used to evaluate data clustering are given as follows, some with reference to Table 5.

Accuracy (ACC)

$$(Acc) = \frac{\sum_i \sum_j \mathbb{1}\{i = j\} n_{ij}}{\mathbf{S}} \quad (3)$$

Normalised Mutual Information (NMI)

$$(NMI) = \frac{2I(\mathbf{X}, \mathbf{Y})}{H(\mathbf{X}) + H(\mathbf{Y})} \quad (4)$$

, where $I(\mathbf{X}, \mathbf{Y})$ is the mutual information between \mathbf{X} and \mathbf{Y} , and $H(\mathbf{X})$ is the entropy of \mathbf{X} .

Rand Index (RI)

$$(RI) = \frac{\binom{N}{2} - \left[\frac{1}{2} \sum_i (\sum_j n_{ij})^2 + \sum_j (\sum_i n_{ij})^2 - \sum_i \sum_j n_{ij}^2 \right]}{\binom{N}{2}} \quad (5)$$

$$= \frac{\alpha + \beta}{\binom{N}{2}}$$

, where α refers to the number of elements that are in the same subset in X and in the same subset in Y , while β is the number of elements that are in different subsets in X and in different subsets in Y .

Adjusted Rand Index (ARI)

$$(ARI) = \frac{\sum_i \sum_j \binom{n_{ij}}{2} - \frac{\sum_i \binom{a_i}{2} \sum_j \binom{b_j}{2}}{\binom{N}{2}}}{\frac{1}{2} \left[\sum_i \binom{a_i}{2} + \sum_j \binom{b_j}{2} \right] - \frac{\sum_i \binom{a_i}{2} \sum_j \binom{b_j}{2}}{\binom{N}{2}}} \quad (6)$$

C Further results

C.1 t-SNE on single-view cancer types

	ACC	NMI	RI	Adj RI
Genomics	0.595 (0.044)	0.299 (0.041)	0.667 (0.017)	0.253 (0.039)
Epigenomics	0.500 (0.036)	0.116 (0.033)	0.598 (0.018)	0.107 (0.035)
Transcriptomics	0.456 (0.023)	0.042 (0.011)	0.572 (0.006)	0.049 (0.013)

Table 6: Clustering performance on the induced embedding of a single view obtained by implementing t-SNE on Cancer Types data. Standard deviation is reported in the parentheses.

Table 6 presents the clustering performance of t-SNE applied on the three views in the Cancer types dataset separately. Genomics was the favoured view on all evaluating measures. It is worth noting that all three views produced better results than a random allocation of the patients into three classes, showing that all views can have a positive influence in determining the cancer type of the patients.

C.2 Handwritten digits projection in 3 dimensions (3D)

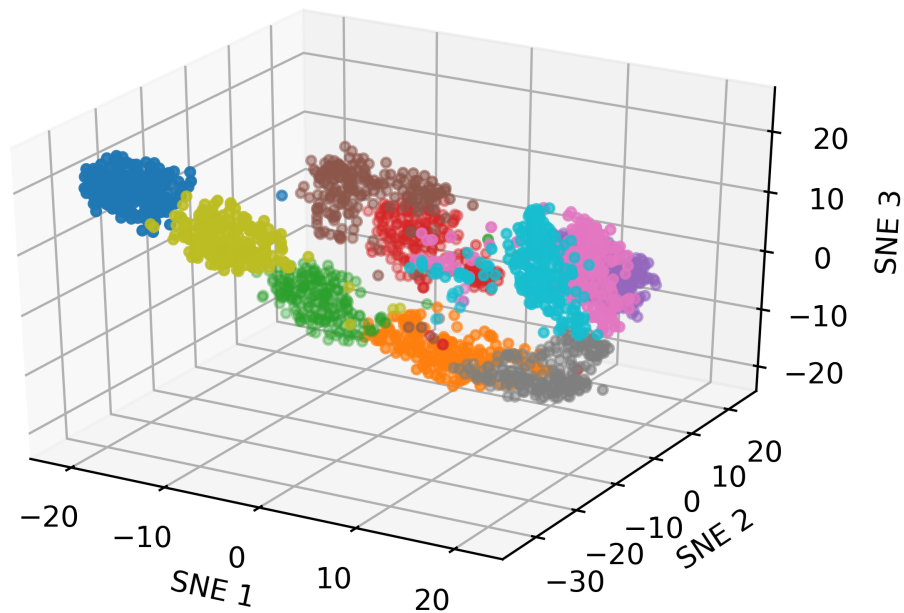


Figure 9: **3D visualisation of handwritten digits.** Produced by multi-SNE with perplexity $P = 80$. Colours present the true clustering on the data points.

D Reproducibility

The code of multi-SNE was based on the publicly available software, written by the author of t-SNE, found in the following link:

<https://lvdmaaten.github.io/tsne/>

We refer the readers to follow the code and functions provided in the link below to reproduce the findings of this paper. The software for m-SNE was not found publicly available and thus we used our own implementation of the method that can be found in the same link below:

https://github.com/theorod93/multiView_manifoldLearning

We refer the readers to follow the links provided in the main body of the paper for the public multi-view data used in this paper.